

# From OTFS to AFDM: A Comparative Study of Next-Generation Waveforms for ISAC in Doubly-Dispersive Channels

Hyeon Seok Rou, *Graduate Student Member, IEEE*,

Giuseppe Thadeu Freitas de Abreu, *Senior Member, IEEE*, Junil Choi, *Senior Member, IEEE*,

David González G., *Senior Member, IEEE*, Marios Kountouris, *Fellow, IEEE*,

Yong Liang Guan, *Senior Member, IEEE*, and Osvaldo Gonsa.

## Abstract

Next-generation wireless systems will offer integrated sensing and communications (ISAC) functionalities not only in order to enable new applications, but also as a means to mitigate challenges such as doubly-dispersive channels, which arise in high mobility scenarios and/or at millimeter-wave (mmWave) and Terahertz (THz) bands. An emerging approach to accomplish these goals is the design of new waveforms, which draw from the inherent relationship between the doubly-dispersive nature of time-variant (TV) channels and the environmental features of scatterers manifested in the form of multipath delays and Doppler shifts. Examples of such waveforms are the delay-Doppler domain orthogonal time frequency space (OTFS) and the recently proposed chirp domain affine frequency division multiplexing (AFDM), both of which seek to simultaneously combat the detrimental effects of double selectivity and exploit them for the estimation (or sensing) of environmental information. This article aims to provide a consolidated and comprehensive overview of the signal processing techniques required to support reliable ISAC over doubly-dispersive channels in beyond fifth generation (B5G)/sixth generation (6G) systems, with an emphasis on OTFS and AFDM waveforms, as those, together with the traditional orthogonal frequency division multiplexing (OFDM) waveform, suffice to elaborate on the most relevant properties of the trend. The analysis shows that OTFS and AFDM indeed enable significantly improved robustness against inter-carrier interference (ICI) arising from Doppler shifts compared to OFDM. In addition, the inherent delay-Doppler domain orthogonality of the OTFS and AFDM effective channels is found to provide significant advantages for the design and the performance of integrated sensing functionalities.

## I. INTRODUCTION

It is expected that beyond fifth generation (B5G) and sixth generation (6G) wireless systems will employ extremely high-frequency (EHF) technologies, operating in the millimeter-wave (mmWave) and Terahertz (THz) bands [1] as a means to support applications [2], such as Internet-of-Things (IoT), edge computing and smart cities; and scenarios such as vehicle-to-everything (V2X), high-speed rail, and non-terrestrial networks (NTNs), which are often subjected to heterogeneous and high-mobility conditions [3]. High-mobility scenarios are known to pose a significant challenge to wireless communications systems due to the resulting doubly-dispersive wireless channel, also referred to as time-variant (TV) multipath, or time-frequency selectivity [4]. Such heterogeneous scattering environments deteriorate the received signal in the form of path delays and Doppler shifts, resulting in inter-symbol interference (ISI) and inter-carrier interference (ICI) which can drastically decrease communication performance under conventional and highly effective modulation schemes, such as orthogonal frequency division multiplexing (OFDM) [5].

Concomitant with this challenge, there is a growing expectation that B5G and 6G systems will offer integrated sensing and communications (ISAC) capabilities, possibly with unified hardware and signal processing techniques [6]. In addition to providing environment perception and accurate/reliable localization information to serve the aforementioned applications, the enhancements introduced by ISAC are fundamental to improve spectrum and energy efficiency, and to lower hardware costs of systems operating in high-mobility scenarios [7].

While it is difficult to foresee which of the upcoming generations/standards – i.e., B5G or 6G – will see ISAC adopted and implemented into commercial systems, the topic is one of the most intensively discussed among pre-standardization fora on wireless systems in recent years<sup>1</sup>, with notable examples being the 6G Smart Networks and Services Industry Association (6G-IA), where ISAC has been identified as a priority technology for its members, and the 5G Automotive Association (5GAA), where ISAC is considered an enabling technology for Cellular-V2X (C-V2X) services. Although it is reasonable to anticipate that any form of practically deployed fifth generation (5G)-based ISAC will likely leverage OFDM, more specifically cyclic prefix (CP)-OFDM and DFT-spread OFDM (DFT-s-OFDM) for down-link/sidelink, and uplink, respectively, but for 6G, new waveforms, such as orthogonal time frequency space (OTFS) and/or affine frequency division multiplexing (AFDM), should be considered to fully exploit the benefits of ISAC. In fact, important standardization bodies such as European Telecommunications Standards Institute (ETSI) and the 3<sup>rd</sup> generation partnership project (3GPP), which produce technical specifications for mobile broadband systems worldwide, have recently added ISAC to their work plans and roadmaps, with ETSI launching a new group dedicated to ISAC in November 2023.

<sup>1</sup>See <https://5gaa.org/> and <https://6g-ia.eu/> for additional information on 5GAA and 6G-IA, respectively.

In line with this trend, novel waveforms have been recently proposed which, thanks to their ability to retain symbol orthogonality under doubly-dispersive conditions, are both robust to high-mobility and advantageous for ISAC, as they inherently enable the estimation of environmental parameters, such as distance and velocity of scatterer objects (i.e., delay and Doppler shifts). One of the most popular methods is OTFS signaling [8], which leverages the inverse symplectic finite Fourier transform (ISFFT) in order to modulate a two-dimensional (2D) grid of information symbols directly in the delay-Doppler domain, gaining great attention for high-mobility B5G systems thanks to its superior performance compared to currently used waveforms such as OFDM [9].

It is easy to show, indeed, that the full delay-Doppler representation of the channel in OTFS inherently conveys the velocity and range information of the scatterers in the form of the respective multipath delays and Doppler shifts, thus implying significant benefits in terms of ISAC. As a consequence, a plethora of OTFS-based ISAC techniques have been proposed to extract the delay and Doppler parameters of the resolvable paths directly from the channel state information (CSI), which have been shown to compete with the sensing performances of OFDM and frequency modulated continuous wave (FMCW) radars, with higher robustness to mobility and achievable capacity [10].

An alternative strategy to design ISAC-friendly and mobility-robust waveforms is to employ chirp-based multicarrier approaches [11]. While the chirp-domain design is attractive due to the inherent spread-spectrum property and potential for full-duplex operations, an important and common drawback of these earlier approaches is the lack of adaptability to the channel delay and Doppler spreads, which is a consequence of the non-parametrizable transforms in their design.

A more recent take on the idea, which seeks to mitigate the latter drawback, is the AFDM waveform [12], which leverages the inverse discrete affine Fourier transform (IDAFT) [13] in order to modulate information symbols into a *twisted* time-frequency domain, yielding the desired delay-Doppler orthogonality while maintaining the necessary flexibility. The optimizable parametrization of AFDM is further accompanied by other desirable properties, such as full diversity guarantee and increased throughput [12], making AFDM a strong candidate of ISAC-enabling waveform for B5G and 6G systems.

This article aims to offer a thorough analysis of the fundamentals and the future of ISAC technology in heterogeneous high-mobility scenarios, in the form of a comprehensive comparison of prominent candidate waveforms, focusing on OTFS and AFDM. The analysis reveals that the novel delay-Doppler orthogonal designs of OTFS and AFDM benefit the signal processing for both communication and sensing functionalities, advocating the integration of the two. These insights may hold significant interest and value not only for academia, but also for standardization engineers across various industry verticals who are increasingly participating in the development of future generations of mobile broadband systems.

The remainder of the article is organized as follows: the fundamental system models and the required ISAC signal processing techniques for the doubly-dispersive wireless channel<sup>2</sup>, emphasizing the inherent transformations between time, frequency, delay, and Doppler dimensions, are described in Section II. In Section III, the signal models of the identified candidate waveforms for B5G/6G ISAC in doubly-dispersive environments are consolidated, highlighting their interrelationships in terms of the multiplexing domain, transmitter structure, and the core *linear canonical transform (LCT)*. In Section IV, we discuss the radar sensing techniques leveraging the identified candidate waveforms in terms of the radar target detection problem (DP) and radar parameter estimation problem (EP), elaborating on signal processing techniques and solutions categorized into correlation-based methods, and direct/indirect CSI-based approaches. In Section V, the candidate waveforms are compared with basis on different key performance indicators (KPIs) for both communications and radar sensing performances, in addition to implications onto hardware implementation, requirements, and potential challenges. Finally, the key insights provided by the article are summarized, and some future directions of the research are identified.

## II. SIGNAL PROCESSING FUNDAMENTALS OF DOUBLY-DISPERSIVE CHANNELS

A long history of research on wireless communications has resulted in the identification and characterization of two fundamental and distinct types of small-scale fading effects, namely frequency- and time-selectivity, also known as time and frequency dispersion, respectively. In particular, an electromagnetic (EM) signal propagated through a given path is subject to a specific *path delay* proportional to the total propagation distance between the transmitter and the receiver, and a *Doppler shift*<sup>3</sup> proportional to the relative velocities among transmitter, receiver, and scatterer, and the carrier frequency.

In a channel with multiple distinguishable propagation paths, the different copies of the originally transmitted signal with varying time delays and Doppler shifts are superposed at the receiver, resulting in interference that impacts on the reliability and performance of the wireless communication link, unless appropriate signal processing techniques are employed. In this section, we first consolidate the fundamental doubly-dispersive channel model with all of its representations in the time, frequency, delay, and Doppler domains, along with the associated transformation methods, followed by the corresponding signal processing mechanisms available to process the received signal, by the efficient representation of the input-output relationship leveraging a circular convolution matrix.

<sup>2</sup>The importance of modelling the doubly-dispersive channel, especially for ISAC applications, is a highly relevant problem currently discussed in both academia and standardization [14].

<sup>3</sup>We remark that in the related literature, and therefore also in this article, the term *Doppler shift* is often used in a broad sense, including spectral shifts of the propagated signal resulting from phenomena other than the actual Doppler effect, such as frequency offsets and low-frequency phase noise at the local oscillators.

### A. The Doubly-Dispersive Channel Model

Consider a wireless channel between a transmitter and receiver with  $P$  resolvable propagation paths, where each  $p$ -th path, with  $p \in \{1, \dots, P\}$ , is respectively described by a corresponding complex fading coefficient  $h_p \in \mathbb{C}$ , path delay,  $\tau_p \in [0, \tau^{\max}]$ , and Doppler shift  $\nu_p \in [-\nu^{\max}, +\nu^{\max}]$ . The corresponding delay and Doppler spreads of such a doubly-dispersive channel are characterized by the maximum delay  $\tau^{\max}$  [s] and the maximum Doppler shift  $\pm\nu^{\max}$  [Hz], such that the channel can be described by the linear time-variant (LTV)<sup>4</sup> relationship between the input and the output signals, most commonly represented as a time-variant impulse response function (TVIRF) in the time-delay domain, given by [4]

$$h(t, \tau) \triangleq \sum_{p=1}^P h_p \cdot e^{j2\pi\nu_p t} \cdot \delta(\tau - \tau_p), \quad (1)$$

where  $j \triangleq \sqrt{-1}$  is the elementary imaginary number,  $t$  and  $\tau$  denote the instantaneous time and path delay, respectively, and  $\delta(x)$  is the unit impulse function defined by  $\delta(x) = 1$  iff  $x = 0$ .

Alternatively, the TVIRF in the time-delay domain can also be represented in other domains by leveraging appropriate linear transforms [13]. For example, the representation in the time-frequency domain is known as time-variant transfer function (TVTF), which is obtained by a Fourier transform (FT) on the TVIRF over the delay domain, i.e.,

$$H(t, f) \triangleq \mathcal{F}_{\tau \rightarrow f}[h(t, \tau)] = \int_{-\infty}^{+\infty} h(t, \tau) \cdot e^{-j2\pi\tau f} d\tau = \sum_{p=1}^P h_p \cdot e^{j2\pi\nu_p t} \cdot e^{-j2\pi\tau_p f}, \quad (2)$$

where  $f$  is the instantaneous frequency and  $\mathcal{F}[\cdot]$  denotes the continuous FT operator.

The TVTF in the time-frequency domain readily highlights both time and frequency dispersion effects of the channel, visible in the two fast-varying exponential terms dependent on the instantaneous time  $t$  and instantaneous frequency  $f$ , respectively at a rate of the Doppler frequency  $\nu_p$  and delay  $\tau_p$  of the corresponding  $p$ -th propagation path, as illustrated in Fig. 1a. Conversely, the Doppler-variant impulse response function (DVIRF) in the delay-Doppler domain is obtained by an FT on the TVIRF over the time domain, that is

$$\gamma(\nu, \tau) \triangleq \mathcal{F}_{t \rightarrow \nu}[h(t, \tau)] = \int_{-\infty}^{+\infty} h(t, \tau) \cdot e^{-j2\pi\nu t} dt = \sum_{p=1}^P h_p \cdot \delta(\nu - \nu_p) \cdot \delta(\tau - \tau_p), \quad (3)$$

where the time- and frequency-selectivity characteristics are observed in the form of unique impulses in the delay-Doppler plane corresponding to each propagation path, as illustrated in Fig. 1b.

<sup>4</sup>The term "linear time-variant (LTV) system" is not to be confused with linear systems with *time-varying delays* – i.e., systems with delay drifts, where  $\tau_p(t)$  – which are also commonly described as LTV. In this article, we only consider time-invariant delays, in compliance with the related literature on doubly-dispersive channels, e.g., [4], [8], [12].

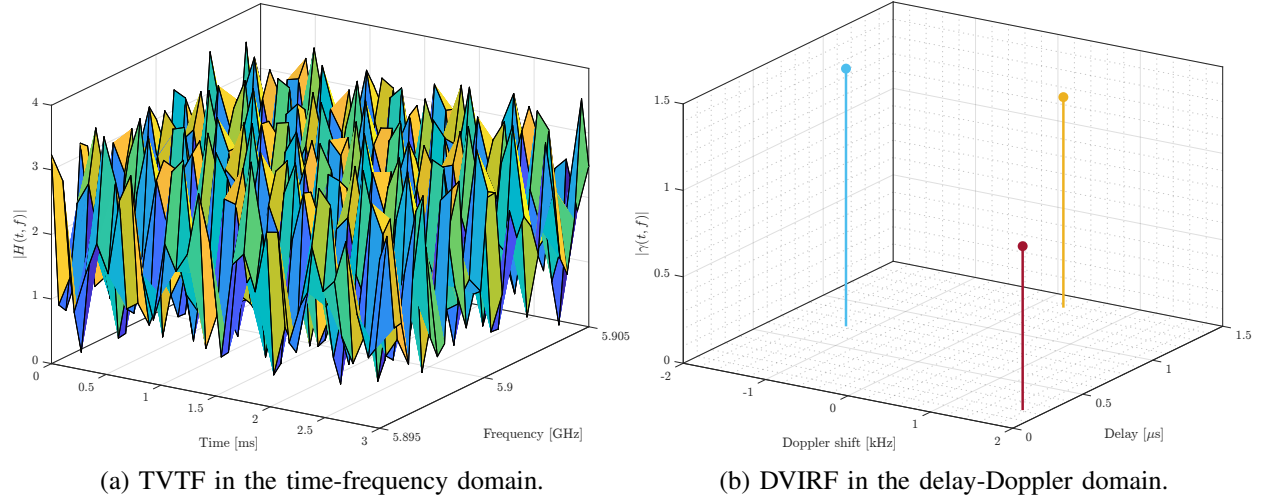


Fig. 1: The doubly-dispersive channel representations with  $P = 3$  resolvable paths, with carrier frequency of 5.9 GHz and signal bandwidth of 10 MHz (following the IEEE 802.11p vehicular environment specifications). The different paths are illustrated by unique colors in Fig. 1b.

Fig. 2 provides a diagram that summarizes the relationships between the various signal domains, including the direction and the integral domain of the necessary linear transforms. Specifically, the rhombus-shaped relationship at the center of the figure illustrates the different domain representations of the doubly-dispersive channel as described above, which also includes the omitted Doppler-variant transfer function (DVTF)<sup>5</sup> in the Doppler-frequency domain.

The Wigner transform (WT) and the Heisenberg transform (HT) (illustrated in red) are generalizations of the multiplexing (MX) and demultiplexing (DMX) operations of the classical OFDM modulator, which transform a 2D time-frequency domain signal into the single time and frequency domains. As will be discussed in the following section, the two transforms can be respectively implemented using the discrete Fourier transform (DFT) and the inverse discrete Fourier transform (IDFT). Furthermore, as can be seen in the figure, there also exist linear transforms that directly describe concatenated FTs and/or inverse Fourier transforms (IFTs). Such linear transforms, such as the symplectic finite Fourier transform (SFFT) and Zak transform (ZT), are leveraged in the transmitter design of next-generation waveforms such as the OTFS [8], and are elaborated in Sec. III.

To wrap up the signal domain fundamentals, let us also address the linear canonical transform (LCT) [13], also known as the affine Fourier transform (AFT), which is a four-parameter transform generalizing<sup>6</sup> many of the popular transforms such as the FT, Laplace transform (LT), and Fresnel transform (fnT).

<sup>5</sup>The Doppler-frequency domain DVTF is not addressed as often compared to the other three forms, due to its lesser intuitive relationship with the physical phenomena. However, it is still an equally valid representation of the doubly-dispersive channel.

<sup>6</sup>Setting specific parameters reduces the LCT to the classical transforms such as  $(0, \frac{1}{2\pi}, -2\pi, 0)$  for the FT,  $(0, \frac{j}{2\pi}, j2\pi, 0)$  for the Laplace transform (LT), and  $(\cos\theta, \frac{1}{2\pi}\sin\theta, -2\pi\sin\theta, \cos\theta)$  to yield the  $\theta$ -th order fractional Fourier transform (frFT).

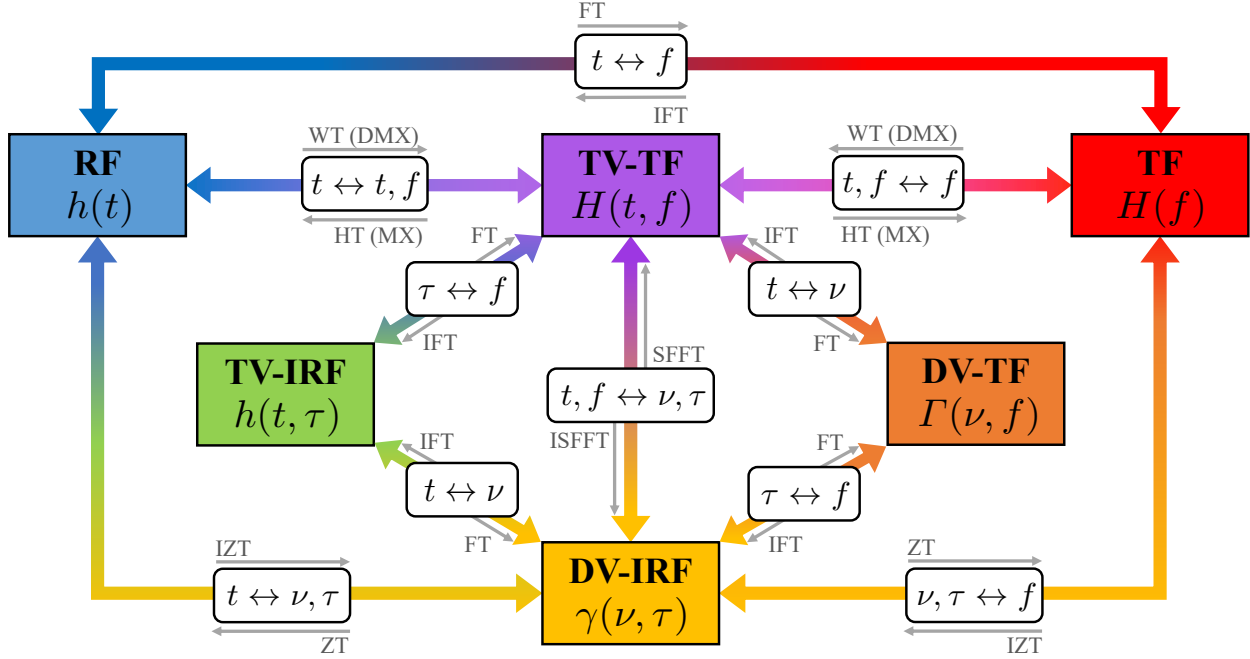


Fig. 2: Illustration of the relationship between the different signal domains and inherent transforms. In addition to the illustrated domains, a special case of the time-frequency domain, namely the **chirp domain**, also exists, which is omitted in this diagram but elaborated upon in the following sections.

In particular, the AFT  $\mathcal{L}_{t \rightarrow u}[\cdot]$  of a time-domain signal  $s(t)$  is described by

$$\mathcal{L}_{t \rightarrow u}[s(t)] \triangleq \begin{cases} \int_{-\infty}^{+\infty} s(t) \cdot \frac{1}{\sqrt{2\pi|b|}} \cdot e^{-j(\frac{a}{2b}u^2 + \frac{1}{b}ut + \frac{d}{2b}t^2)} dt, & b \neq 0, \\ s(d \cdot u) \cdot \frac{1}{\sqrt{a}} \cdot e^{-j\frac{cd}{2}u^2} & b = 0, \end{cases} \quad (4)$$

where the four AFT parameters ( $a, b, c, d$ ) are arbitrary complex scalars satisfying  $ad - bc = 1$ .

As shall be seen, the available degrees-of-freedom (DoF)s of the AFT are exploited by another promising waveform, AFDM [12], which allows for the optimization of the AFT parameters based on the channel statistics in order to ensure the orthogonality of the signal in doubly-dispersive systems.

### B. Input-Output Relationship of Doubly-Dispersive Channel

The input-output relation of the doubly-dispersive wireless channel in time is classically described by the linear convolution over the delay domain, leveraging the TVIRF representation [4], namely

$$r(t) = s(t) * h(t, \tau) + w(t) \triangleq \int_{-\infty}^{+\infty} s(t - \tau) \left( \sum_{p=1}^P h_p \cdot e^{j2\pi\nu_p t} \cdot \delta(\tau - \tau_p) \right) d\tau + w(t), \quad (5)$$

where  $r(t)$ ,  $s(t)$ , and  $w(t)$  are respectively the received signal, input signal, and additive white Gaussian noise (AWGN) in time, while  $*$  denotes the linear convolution operator.

In turn, the discrete equivalent of eq. (5) is given by

$$r[n] = \sum_{\ell=0}^{\infty} s[n-\ell] \left( \sum_{p=1}^P h_p \cdot e^{j2\pi \frac{\nu_p}{f_s} n} \cdot \delta\left(\ell - \frac{\tau_p}{\Delta\tau}\right) \right) + w[n], \quad (6)$$

where  $r[n]$  and  $s[n]$  are respectively the sampled sequences of  $r(t)$  and  $s(t)$  at a sampling rate of  $f_s \triangleq \frac{1}{T_s}$  [Hz], with sampling interval  $T_s$  [s];  $n \in \{0, \dots, N-1\}$  is the sample index; and  $\ell \triangleq \frac{\tau}{T_s}$  is the normalized delay with delay resolution  $T_s$ .

We further introduce the normalized digital Doppler shift and normalized delay of the  $p$ -th propagation path as  $f_p \triangleq \frac{N\nu_p}{f_s}$  and  $\ell_p \triangleq \frac{\tau_p}{T_s}$ , where the delay resolution  $T_s$  is assumed to be sufficiently high, such that the normalized delay  $\ell$  can be rounded to the nearest integer with negligible error, *i.e.*,  $\ell_p - \lfloor \frac{\tau_p}{T_s} \rfloor \approx 0$ . In practical multicarrier wireless communications techniques, the transmit sequence in eq. (6) is prepended with a CP to mitigate the effects of time dispersion. The prefix sequence is defined within a CP length of  $N_{cp}$  samples, such that

$$s[n'] = s[N - n'] \cdot e^{j2\pi \cdot \phi_{cp}(n')}, \quad (7)$$

where  $n' \in \{1, \dots, N_{cp}\}$ , and  $\phi_{cp}(n')$  is a function denoting the multiplicative phase term specific for each waveform, which is set to zero if the CP does not require a phase offset, as in the OFDM.

The CP as described in eq. (7) enables the linear convolutional input-output relation of the TVIRF to be processed as a circular convolutional response. After removing the received signal parts corresponding to the CP, the circular convolutional input-output relationship can be described in matrix form as

$$\mathbf{r} \triangleq \mathbf{H} \cdot \mathbf{s} = \left( \sum_{p=1}^P h_p \cdot \mathbf{\Phi}_p \cdot \mathbf{W}^{f_p} \cdot \mathbf{\Pi}^{\ell_p} \right) \cdot \mathbf{s} + \mathbf{w} \in \mathbb{C}^{N \times 1}, \quad (8)$$

where  $\mathbf{r} \in \mathbb{C}^{N \times 1}$ ,  $\mathbf{s} \in \mathbb{C}^{N \times 1}$ , and  $\mathbf{w} \in \mathbb{C}^{N \times 1}$  are respectively the vectors representing the received signal, the transmit signal, and AWGN;  $\mathbf{H} \in \mathbb{C}^{N \times N}$  is the circular convolution effective channel matrix;  $\mathbf{\Phi}_p \in \mathbb{C}^{N \times N}$  is the diagonal matrix corresponding to the  $p$ -th delayed CP phase as given in eq. (9);  $\mathbf{W} \in \mathbb{C}^{N \times N}$  is the diagonal matrix containing the  $N$ -th roots of unity as given in eq. (10); and  $\mathbf{\Pi} \in \mathbb{C}^{N \times N}$  is the forward cyclic shift matrix obtained by left-shifting the  $N \times N$  identity matrix once, such that  $\mathbf{\Pi}^{\ell_p}$  corresponds to a left-shift operation of a matrix by  $\ell_p \in \mathbb{N}_0$  indices.

As can be seen in eq. (8), the input-output relationship of a doubly-dispersive channel is described by

---


$$\mathbf{\Phi}_p \triangleq \text{diag} \left( \overbrace{\left[ e^{-j2\pi \cdot \phi_{cp}(\ell_p)}, e^{-j2\pi \cdot \phi_{cp}(\ell_p-1)}, \dots, e^{-j2\pi \cdot \phi_{cp}(2)}, e^{-j2\pi \cdot \phi_{cp}(1)} \right]}^{\ell_p \text{ terms}}, \overbrace{\left[ 1, 1, \dots, 1, 1 \right]}^{N-\ell_p \text{ ones}} \right) \in \mathbb{C}^{N \times N}. \quad (9)$$

$$\mathbf{W} \triangleq \text{diag} \left( \left[ 1, e^{-j2\pi/N}, \dots, e^{-j2\pi(N-2)/N}, e^{-j2\pi(N-1)/N} \right] \right) \in \mathbb{C}^{N \times N}. \quad (10)$$



a matrix  $\mathbf{H}$  consisting of  $P$  off-diagonals, whose shifted positions are determined by the integer delay of each path. In addition, the complex values along each diagonal contain the channel fading coefficient and the phase offset information of the delayed CP and the Doppler shift of each path. As a consequence of the circulant convolutional channel structure, the different paths are only resolvable in the delay domain and not in the Doppler domain. Therefore, a key design objective of a double-dispersion robust waveform must be the ability to orthogonalize the delays and Doppler shifts of the channel via means of novel domain transforms in the modulation and demodulation of the transmit signal.

### III. SIGNAL MODELS OF NEXT-GENERATION WAVEFORMS

In this section, we provide the signal models and the transmitter structures of the various waveforms proposed for high performance in the doubly-dispersive channel. First, the OFDM waveform is described as a reference, followed by the next-generation waveform candidates, namely, OTFS, and AFDM, in addition to various derivative waveforms that can be related to the latter.

#### A. Orthogonal Frequency Division Multiplexing (OFDM)

The well-known OFDM transmitter modulates digital symbols from the frequency domain into a time domain signal employing an IDFT operation, as illustrated in Fig. 2. Namely, given a vector  $\mathbf{x} \in \mathbb{C}^{N \times 1}$  consisting of  $N$  complex symbols, the OFDM transmit signal  $\mathbf{s}^{\text{OFDM}} \in \mathbb{C}^{N \times 1}$  is given by [15]

$$\mathbf{s}^{\text{OFDM}} = \mathbf{F}_N^{-1} \cdot \mathbf{x} \in \mathbb{C}^{N \times 1}, \quad (11)$$

where  $\mathbf{F}_N \in \mathbb{C}^{N \times N}$  is the  $N$ -point DFT matrix, and hence  $\mathbf{F}_N^{-1} \triangleq \mathbf{F}_N^H$  is the  $N$ -point IDFT matrix.

Following the above, the received signal  $\mathbf{y}^{\text{OFDM}} \in \mathbb{C}^{N \times 1}$  over the circular convolutional channel described by eq. (8) is demodulated via the forward  $N$ -point DFT, i.e.,

$$\mathbf{y}^{\text{OFDM}} = \mathbf{F}_N \overbrace{(\mathbf{H} \cdot \mathbf{s}^{\text{OFDM}} + \mathbf{w})}^{\triangleq \mathbf{r}^{\text{OFDM}} \in \mathbb{C}^{N \times 1}} = \overbrace{(\mathbf{F}_N \cdot \mathbf{H} \cdot \mathbf{F}_N^{-1})}^{\triangleq \mathbf{G}^{\text{OFDM}} \in \mathbb{C}^{N \times N}} \mathbf{x} + \mathbf{F}_N \cdot \mathbf{w} \in \mathbb{C}^{N \times 1}, \quad (12)$$

where, for exposition convenience, we defined the OFDM receive signal as  $\mathbf{r}^{\text{OFDM}} \in \mathbb{C}^{N \times 1}$ , and the effective channel  $\mathbf{G}^{\text{OFDM}} \in \mathbb{C}^{N \times N}$  describing the input-output relationship of the baseband OFDM symbols, which can be obtained by combining eqs. (8) and (12) to yield

$$\mathbf{G}^{\text{OFDM}} \triangleq \sum_{p=1}^P h_p \cdot \mathbf{F}_N \left( \Phi_p \cdot \mathbf{W}^{f_p} \cdot \Pi^{\ell_p} \right) \mathbf{F}_N^H. \quad (13)$$

As illustrated in Fig. 3, the column-wise DFT and row-wise IDFT in the presence of Doppler shifts cause the channel diagonals of the convolution matrix to be spread into a decaying band, centered at the original diagonals, such that significant interference between each path may arise.

### B. Orthogonal Time Frequency Space (OTFS)

In the OTFS modulation scheme, the information symbols are first directly placed in the delay-Doppler domain, instead of the frequency domain as in the OFDM approach, which are then multiplexed into the time signal. Namely, the complex baseband symbols are structured into a 2D grid of size  $K \times L$  in the delay-Doppler domain, which are first transformed into the time-frequency domain via the ISFFT, and then into the continuous time signal via a pulse-shaping HT. As illustrated in Fig. 2, such a two-step OTFS domain transformation process can also be achieved via a single inverse discrete Zak transform (IDZT), which is an alternative and equivalent representation of the OTFS modulation process [8]. For the sake of clarity, however, we will hereafter adopt the ISFFT formulation, known to be implemented via DFTs/IDFTs.

In light of the above, the OTFS modulation process can be described mathematically as

$$\mathbf{s}^{\text{OTFS}} \triangleq \text{vec} \left( \overbrace{\mathbf{P}^{\text{tx}} \mathbf{F}_K^{-1}}^{\text{Pulse-shaping HT}} \cdot \overbrace{(\mathbf{F}_K \mathbf{X} \mathbf{F}_L^{-1})}^{\text{ISFFT}} \right) = (\mathbf{F}_L^{-1} \otimes \mathbf{P}^{\text{tx}}) \cdot \overbrace{\text{vec}(\mathbf{X})}^{\triangleq \mathbf{x}} \in \mathbb{C}^{KL \times 1}, \quad (14)$$

where  $\mathbf{s}^{\text{OTFS}} \in \mathbb{C}^{KL \times 1}$  is the OTFS transmit signal vector,  $\mathbf{X} \in \mathbb{C}^{K \times L}$  is the information symbol matrix consisting of  $N \triangleq KL$  number of complex symbols<sup>7</sup>,  $\mathbf{P}^{\text{tx}} \in \mathbb{C}^{K \times K}$  is the diagonal transmit pulse-shaping filter matrix,  $\mathbf{F}_K \in \mathbb{C}^{K \times K}$  and  $\mathbf{F}_L \in \mathbb{C}^{L \times L}$  are the  $K$ -point and  $L$ -point DFT matrices, and  $\text{vec}(\cdot)$  and  $\otimes$  denote the stacking vectorization and Kronecker product operators, respectively.

The filtered and demodulated signal  $\mathbf{y}^{\text{OTFS}}$  after the convolution channel  $\mathbf{H}$  in eq. (8) is given by

$$\mathbf{y}^{\text{OTFS}} \triangleq (\mathbf{F}_L \otimes \mathbf{P}^{\text{rx}}) \overbrace{(\mathbf{H} \cdot \mathbf{s}^{\text{OTFS}} + \mathbf{w})}^{\triangleq \mathbf{r}^{\text{OTFS}} \in \mathbb{C}^{KL \times 1}} = \mathbf{G}^{\text{OTFS}} \cdot \mathbf{x} + (\mathbf{F}_L \otimes \mathbf{P}^{\text{rx}}) \cdot \mathbf{w} \in \mathbb{C}^{KL \times 1}, \quad (15)$$

where  $\mathbf{P}^{\text{rx}} \in \mathbb{C}^{K \times K}$  is the diagonal matched filter matrix of  $\mathbf{P}^{\text{tx}}$ , and the effective OTFS channel  $\mathbf{G}^{\text{OTFS}} \in \mathbb{C}^{N \times N}$  in the delay-Doppler domain is given by

$$\mathbf{G}^{\text{OTFS}} \triangleq \sum_{p=1}^P h_p \cdot (\mathbf{F}_L \otimes \mathbf{P}^{\text{rx}}) \left( \Phi_p \cdot \mathbf{W}^{f_p} \cdot \Pi^{\ell_p} \right) (\mathbf{F}_L^H \otimes \mathbf{P}^{\text{tx}}) \in \mathbb{C}^{N \times N}, \quad (16)$$

which is the convolutional channel matrix  $\mathbf{H}$  after a block-wise pulse-shaped<sup>8</sup> DFT and IDFT.

It can be observed from eq. (16) that the  $KL = N$  elements in each diagonal of the convolutional matrix of eq. (8) are spread into the OTFS effective channel via the block-wise pulse-shaping FTs, such that the  $KL \times KL$  OTFS channel matrix can be considered as a  $K \times K$  grid of  $L \times L$  sub-matrices (illustrated as minor grids in Fig. 3). In light of the above, the positions of the non-zero channel coefficient

<sup>7</sup>Without loss of generality, we assume  $N \triangleq KL$  to enable direct comparison with 1D modulation schemes, i.e., OFDM.

<sup>8</sup>The literature commonly assumes rectangular OTFS pulses [8], which reduces  $\mathbf{P}^{\text{tx}}$  and  $\mathbf{P}^{\text{rx}}$  to  $K \times K$  identity matrices.

elements can be deterministically obtained by the values of both delay and Doppler shift of each path, respective to the occupied sub-matrices and the amount of left-shift of the diagonals.

For the integer Doppler shift model, each path occupies exactly  $K$  sub-matrices out of the  $K \times K$  grid in a shifted block-diagonal structure, such that the amount of right-shift is determined by the integer value of the Doppler shift,  $f_p^{\text{int}} \triangleq \lfloor f_p \rfloor$ . For example, a path with  $f_p^{\text{int}} = 0$  occupies the  $K$  sub-matrices in the main block-diagonal (shift of index 0), whereas a path with  $f_p^{\text{int}} = 1$  occupies the  $K$  sub-matrices in the block-diagonal, which is right-shifted by an index of 1. On the other hand for negative Doppler shifts, the block-diagonals are left-shifted by an index of  $\lfloor f_p^{\text{int}} \rfloor$ , as illustrated by path 3 in Fig. 3a.

In turn, each of the  $K$  occupied sub-matrices follows the same structure consisting of exactly  $L$  non-zero elements in a shifted diagonal, with a left-shift relative to the main diagonal determined by the value of the path delay  $\ell_p$ . For example, for a path with delay  $\ell_p = 0$ , the  $L$  non-zero elements are placed in the main diagonal for all  $K$  sub-matrices, whereas a path with  $\ell_p = 3$  will have the  $L$  non-zero elements in the diagonal left-shifted by three indices, for all  $K$  sub-matrices<sup>9</sup>.

It follows that the OTFS waveform can achieve orthogonality and resolvability in the delay-Doppler domain with integer delay and integer Doppler shifts, given  $\ell^{\text{max}} \leq L - 1$  and  $f^{\text{max}} \leq \lfloor \frac{K}{2} \rfloor$ , where  $\ell^{\text{max}} \triangleq \lceil \frac{\tau^{\text{max}}}{\Delta\tau} \rceil$  and  $f^{\text{max}} \triangleq \lfloor \frac{N\nu^{\text{max}}}{f_s} \rfloor$  are the maximum normalized delay and Doppler shift.

In contrast, in the case of **fractional** Doppler, the powers of the channel elements are diffused (or "leaked") across all  $K^2$  sub-matrices over the main  $K$  block-diagonal sub-matrices of the integer case, resulting in a Doppler domain interference as illustrated in Fig. 3b and Fig. 3c. The amount of such power leakage is determined by the value of the fractional part of the Doppler shift given by  $f_p^{\text{frac}} \triangleq f_p - f_p^{\text{int}} \in [0.5, +0.5)$ , such that larger fractional parts result in more leakage.

### C. Affine Frequency Division Multiplexing (AFDM)

In AFDM, a one-dimensional vector of symbols  $\mathbf{x} \in \mathbb{C}^{N \times 1}$  is directly multiplexed into a *twisted* time-frequency chirp domain using the IDAFT [16], as described by

$$\mathbf{s}^{\text{AFDM}} \triangleq \mathbf{A}^{-1} \cdot \mathbf{x} = \overbrace{(\mathbf{\Lambda}_{c_2} \cdot \mathbf{F}_N \cdot \mathbf{\Lambda}_{c_1})^{-1}}^{\text{IDAFT}} \cdot \mathbf{x} = (\mathbf{\Lambda}_{c_1}^H \cdot \mathbf{F}_N^H \cdot \mathbf{\Lambda}_{c_2}^H) \cdot \mathbf{x} \in \mathbb{C}^{N \times 1}, \quad (17)$$

where  $\mathbf{A} \triangleq \mathbf{\Lambda}_{c_2} \mathbf{F}_N \mathbf{\Lambda}_{c_1} \in \mathbb{C}^{N \times N}$  is the forward  $N$ -point discrete affine Fourier transform (DAFT) matrix, and  $\mathbf{\Lambda}_{c_i} \triangleq \text{diag}[e^{-j2\pi c_i(0)^2}, \dots, e^{-j2\pi c_i(N-1)^2}] \in \mathbb{C}^{N \times N}$  is a diagonal chirp matrix with a central digital frequency of  $c_i$ .

<sup>9</sup>A Matlab<sup>®</sup> implementation of the doubly-dispersive channel model described in this Section, as well as a convenient visualization tool used to generate some of the figures can be found our online repository [*here*].

It follows that the demodulated AFDM signal over the convolution channel in eq. (8) is given by

$$\mathbf{y}^{\text{AFDM}} = \mathbf{A} \cdot \overbrace{(\mathbf{H} \cdot \mathbf{s}^{\text{AFDM}} + \mathbf{w})}^{\triangleq \mathbf{r}^{\text{AFDM}} \in \mathbb{C}^{N \times 1}} = \mathbf{G}^{\text{AFDM}} \cdot \mathbf{x} + \mathbf{A} \cdot \mathbf{w} \in \mathbb{C}^{N \times 1}, \quad (18)$$

with the effective AFDM channel given by

$$\mathbf{G}^{\text{AFDM}} \triangleq \sum_{p=1}^P h_p \cdot (\mathbf{\Lambda}_{c_2} \cdot \mathbf{F}_N \cdot \mathbf{\Lambda}_{c_1}) \left( \mathbf{\Phi}_p \cdot \mathbf{W}^{f_p} \cdot \mathbf{\Pi}^{\ell_p} \right) (\mathbf{\Lambda}_{c_1}^H \cdot \mathbf{F}_N^H \cdot \mathbf{\Lambda}_{c_2}^H) \in \mathbb{C}^{N \times N}, \quad (19)$$

where the central frequencies  $c_1$  and  $c_2$  of the two diagonal chirps<sup>10</sup> can be optimized to the channel statistics to improve the orthogonality of the diagonals of the AFDM effective channel.

The AFDM effective channel achieves full orthogonality in the integer delay-Doppler domain when the orthogonality condition is satisfied, which is given by

$$2(f^{\max} + \xi)(\ell^{\max} + 1) + \ell^{\max} \geq N, \quad (20)$$

where  $\xi \in \mathbb{N}$  is a free parameter determining the so-called *guard width* of the AFDM, denoting the number of additional guard elements around the diagonals to anticipate for Doppler-domain interference.

Assuming the latter orthogonality condition is met, the AFDM chirp frequencies are obtained by

$$c_1 = \frac{2(f^{\max} + \xi) + 1}{2N}, \quad \text{and} \quad c_2 \ll \frac{1}{N}, \quad (21)$$

where the flexibility in  $c_2$  enables fine-tuning of the waveform shape as will be discussed in Sec. IV.

In light of the above, the position of the shifted diagonal in the AFDM channel can also be described in terms of the delay-Doppler indices of each path. Unlike the intricate block-wise structure of the OTFS effective channel, the AFDM effective channel exhibits only a single diagonal per path, which is shifted by a deterministic index dependent on the integer delay and integer Doppler shift. In other words, each diagonal of the convolution channel in eq. (8) is right-shifted by an index of exactly  $\ell_p \cdot 2(f^{\max} + \zeta) + f_p^{\text{int}}$  positions, as illustrated in Fig. 3a. On the other hand, in the presence of fractional Doppler shifts, the diagonals of the AFDM effective channels also exhibit power leakage around the main diagonal, resulting in Doppler-domain interference as can be seen in Figs. 3b and 3c.

<sup>10</sup>It is shown in [12] that the chirp frequencies  $c_1$  and  $c_2$  are actually correspondent to the four configurable parameters of the AFT formulation in eq. (4).

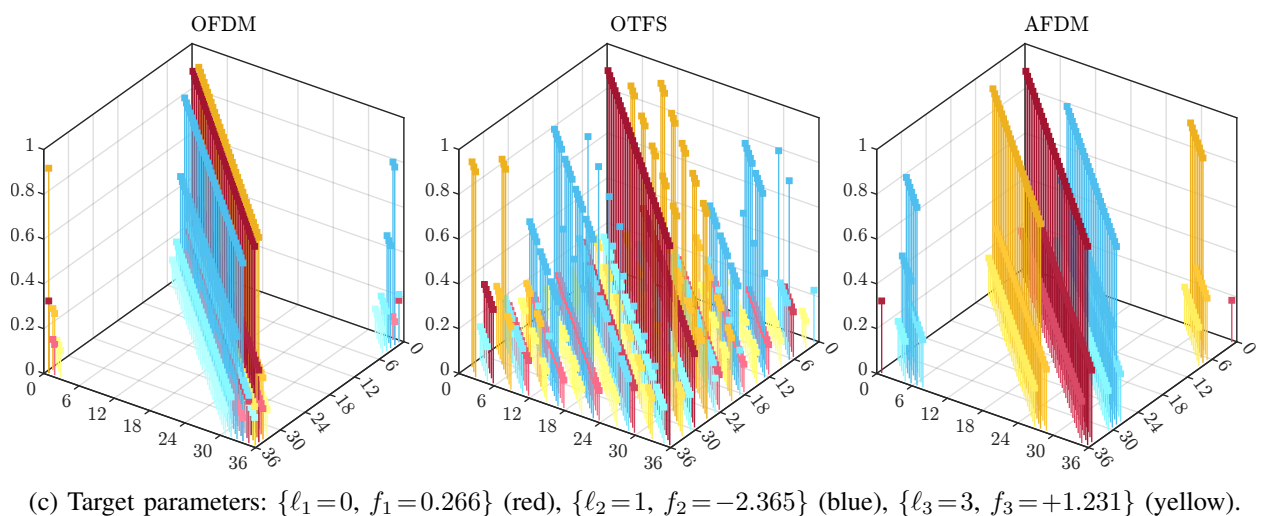
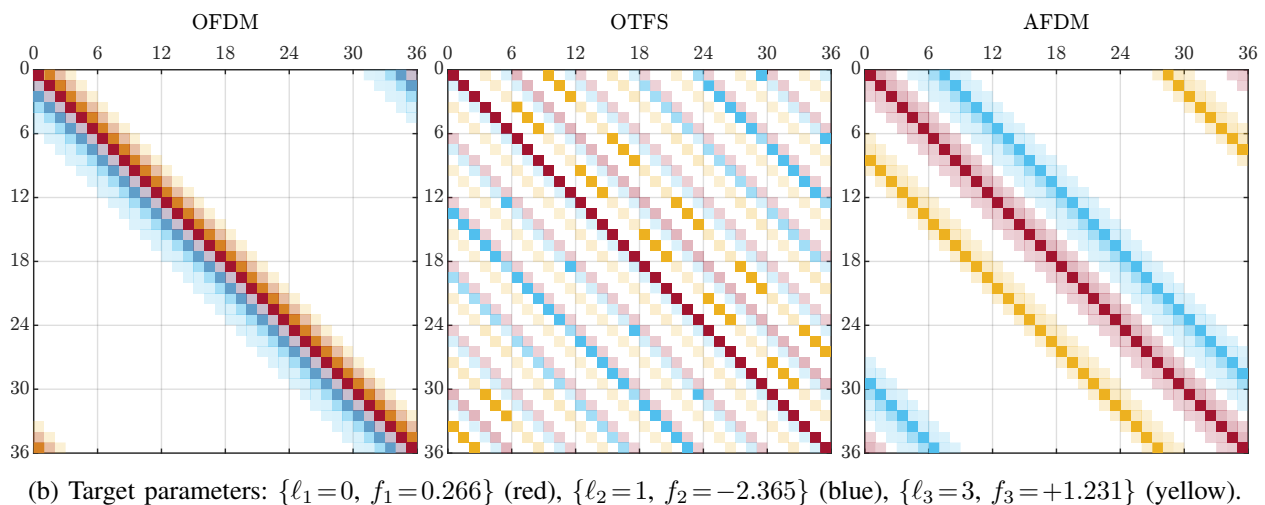
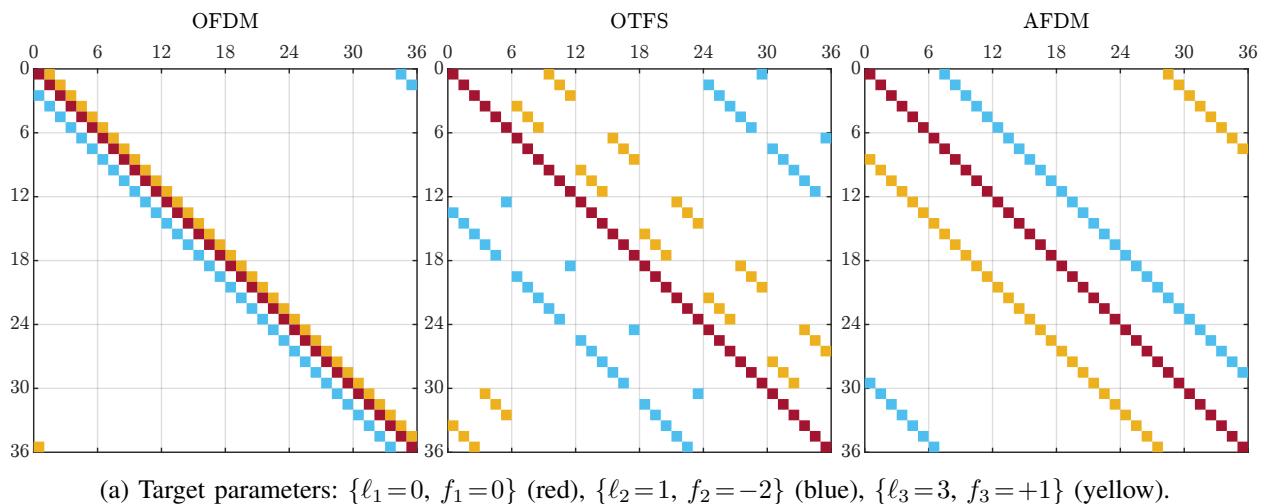


Fig. 3: Effective channel matrix structures of different waveforms in a doubly-dispersive channel with  $P = 3$  resolvable paths (each depicted in a different color), with corresponding normalized delays  $\ell_p$  and normalized digital Doppler shifts  $f_p$ . The system size parameters are  $N = 36$  for the OFDM and AFDM, and  $K = 6, L = 6$  for the OTFS. The fading colors for the fractional Doppler case correspond to the magnitude of the elements whereas darker colors correspond to larger powers. Channel components with a magnitude lower than  $1/2N$  are considered negligible and not visualized in the figure.

#### D. Related Next-Generation Waveforms

In this section, we briefly discuss various waveforms which, as illustrated in Fig. 4 and put into a chronological context in Fig. 5, are related to the aforementioned OFDM, OTFS, and AFDM, and can also be potential candidates to support ISAC in B5G/6G systems. Due to space limitation, however, the discussion is resumed to a qualitative comparison, addressed in more detail in Sec. III.

1) *Intermediate Chirp Domain Waveforms*: A few chirp-domain waveforms also exist, which in commonality with OFDM and AFDM, aim at orthogonalizing delay and Doppler shift indices. Such waveforms, which include orthogonal chirp division multiplexing (OCDM) [11] and DAFT-OFDM [17], can be seen as special cases of AFDM, with non-ideal and simplified chirp frequencies  $c_1$  and  $c_2$  [12], naturally exhibiting equal or worse performances depending on the doubly-dispersive channel profile.

2) *Enhanced Delay-Doppler Waveforms*: Various methods adopt the novel delay-Doppler signal representation of OTFS, and have proposed enhanced delay-Doppler domain waveforms. Examples are the transcendentially-rotated OTFS (T-OTFS) [18], which maximizes the asymptotic diversity of OTFS via a phase-rotating precoder; orthogonal time sequency modulation (OTSM) modulation [19], which seeks to reduce implementation complexity by leveraging a new type of domain transform; and orthogonal delay-Doppler division multiplexing (ODDM) [20], which improves upon OTFS via an optimized pulse-shaping filter that creates feasible pulses that are orthogonal with respect to the delay-Doppler plane resolution.

3) *Filter Bank-based (Pulse-Shaping) Waveforms*: Finally, various multicarrier techniques leverage optimized pulse-shaping filter banks, such as filter bank multi-carrier (FBMC) [21] and generalized frequency division multiplexing (GFDM) [22], which improve the out-of-band (OOB) emissions, spectral efficiency, ISI, and ICI problems of OFDM via robust adaptation of the subcarriers and modulation pulses with respect to the doubly-dispersive channel statistics.

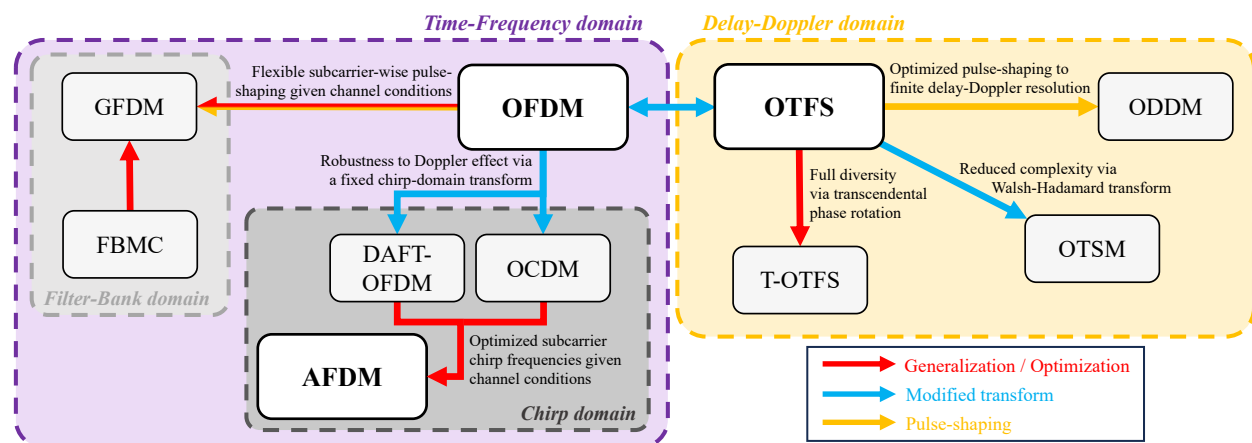


Fig. 4: A map of relationships between next-generation waveforms and their signal domains.

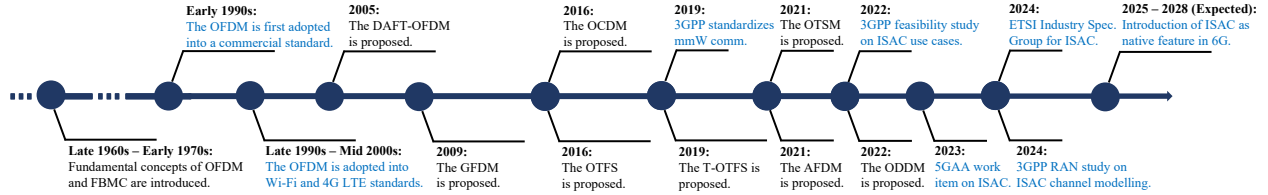


Fig. 5: Timeline highlighting the invention of various waveforms, and key dates in standardization.

#### IV. INTEGRATED SENSING AND COMMUNICATIONS (ISAC) USING NEXT-GENERATION WAVEFORMS

In ISAC, wireless “sensing” refers to the ability to harness the rich information about the surrounding environment inherently embedded in radio signals affected by channel conditions. Drawing a parallel with well-established *radar* technologies [23] two distinct types of sensing problems can therefore be identified, namely: 1) the **detection problem (DP)**, which relates to resolving the number of unique scattering points of interest (targets) from the background clutter, and 2) the **estimation problem (EP)**, which refers to extracting parameters such as range, velocity, and bearing associated with the aforementioned targets.

Considering a single-antenna monostatic sensing scenario, where the transmitter and the receiver are colocated<sup>11</sup>, the scatterer (target) range  $r$  [m] and the relative linear velocity  $v$  [m/s] are related to the round-trip delay  $\tau$  and Doppler shift  $\nu$  of the echo signal by

$$\tau \triangleq \frac{2r}{c}, \quad \text{and} \quad \nu \triangleq \frac{2v f_c}{c}, \quad (22)$$

where  $c$  is the speed of light and  $f_c$  is the carrier frequency of the transmitted signal.

For the sake of simplicity, we address here only the single-input single-output (SISO) system model, as the multiple-input multiple-output (MIMO) extension can be trivially derived by leveraging array response vectors and the corresponding signal processing techniques [25]. This enables the estimation of bearing, and in the case of planar arrays, the azimuth and elevation angles of the target in 3D space.

Solutions to the DPs and EPs can be further classified into **three methods** based on their approaches: a) **correlation-based** methods, in which echo signals are filtered with a known transmit signal in order to yield radar parameter estimates; b) **direct CSI-based** methods, where radar parameters are extracted *a posteriori* from the known channel matrix; and c) **indirect CSI-based** methods, where radar parameters estimation and CSI acquisition are performed jointly, by leveraging the known channel structure. Each of these approaches is discussed further in the sequel.

<sup>11</sup>The bistatic scenario with distributed radar transmitter and receiver can also be considered for several applications and use cases [24], where the estimated channels may be non-reciprocal. This scenario is beyond the scope of this article but is an important setting to be addressed in future work, which can enable the full potential of ISAC.

### A. Correlation-based Methods

Classical radar systems based on chirps and impulsive waveforms [23] are typical examples of the correlation-based method, as the received echo signals are processed by a correlation (matched filter) with a known probing signal, to directly yield the target parameters. Radar waveforms are, however, optimized to exhibit correlation properties that can achieve high resolution in the delay and Doppler domains, which is generally not possible to do with communication waveforms without sacrificing communication objectives (e.g., rate, efficiency, latency, etc.).

The fundamental resolution of the correlation-based method can be analyzed through the well-known 2D ambiguity function of a waveform in delay-Doppler domain<sup>12</sup>, which is given by

$$A(\tau, \nu) \triangleq \int_{-\infty}^{+\infty} s(t) \cdot s^*(t - \tau) \cdot e^{j2\pi\nu t} dt, \quad (23)$$

where  $A(\tau, \nu)$  is the 2D ambiguity function parametrized by the delay and Doppler shift values,  $s(t)$  is the transmit signal, and  $(\cdot)^*$  denotes the complex conjugation operation.

By inspecting the ambiguity function behaviors of the OFDM, OTFS, and AFDM waveforms [26], the different delay-Doppler resolution and beamlobe behaviors of the waveforms can be observed. Namely, it is found that that OFDM shows high resolution in the delay domain, but not in Doppler, whereas OTFS and AFDM show moderate resolution in both domains simultaneously, with AFDM exhibiting an adjustable mainlobe width with a trade-off in the two domains by leveraging the chirp frequency parameters  $c_1$  and  $c_2$ . Therefore naturally, correlation-based estimators of low complexity, employing OFDM, OTFS, and AFDM [26]–[28], have been proposed, but were found to be still fundamentally dependent on the resolution of the ambiguity function, promoting subsequent development of parameter estimation methods based on the higher resolution of the inherent delay-Doppler modulation grid.

### B. Direct CSI-based Methods

These methods operate under the assumption that channel estimation has been performed such that the channel matrix is available, and aim to extract radar parameters *a posteriori*, by exploiting the deterministic structure of the doubly-dispersive channel as described in Sec. III, which is dependent on the target delay and Doppler shift parameters. Several sensing algorithms based on this approach have been proposed. Assuming that CSI is obtained in the time-frequency domain as per eq. (2), the resulting estimation problem on  $\tau_p$  and  $\nu_p$  is referred to as a multidimensional harmonic retrieval problem, to which many well-known super-resolution solutions exist, such as MULTiple Signal Classification (MUSIC) and estimation of signal parameters via rotational invariance techniques (ESPRIT), in addition to enhanced

<sup>12</sup>In the case for MIMO, the ambiguity function is extended into three-dimensional (3D) including the angular domain.



tensor-based algorithms in the case of MIMO scenarios with increased dimensionality, as discussed in [6]. The approach is known to achieve high resolution and accuracy but typically requires a large number of continuously obtained observation samples, which together with the fundamental dependence on the channel estimation performance, constitute a prominent challenge of such methods, since channel estimation errors may propagate to the radar parameter estimates.

Setting these issues aside, with a sufficiently large number of observations and appropriate filtering, the effective channel matrices of the waveforms as given in eqs. (13), (16), and (19) may be obtained via compressive sensing and other matrix reconstruction algorithms. In such cases, the delay-Doppler orthogonality of the OTFS and AFDM effective channels, in addition to the injective mapping between each integer delay-Doppler pair and the position of the shifted-diagonal as discussed in Sec. III, enable efficient extraction of the target parameters from the channel matrix element positions. However, in the presence of fractional Doppler shifts, the resulting interference in the Doppler domain illustrated in Fig. 3b can significantly deteriorate such "position-based" methods in terms of Doppler resolution.

### C. Indirect CSI-based Methods (Integrated Channel Estimation)

In cases where the channel matrix is not available but its structure is known, an optimization problem can be formulated to jointly estimate the channel inherently incorporating the radar parameters, yielding an integrated channel and target parameter estimation. For instance, the following minimization problem can be formulated and solved

$$\underset{\tau_p, \nu_p, h_p, \forall p}{\operatorname{argmin}} \mathcal{L}(\mathbf{r} - \tilde{\mathbf{H}}(\tau_p, \nu_p, h_p; \forall p) \cdot \mathbf{s}), \quad (24)$$

where  $\mathbf{r} \triangleq \mathbf{H}\mathbf{s} + \mathbf{w} \in \mathbb{C}^{N \times 1}$  is the received signal,  $\tilde{\mathbf{H}}(\tau_p, \nu_p, h_p; \forall p) \in \mathbb{C}^{N \times N}$  is the estimated channel parametrized by the  $3P$  radar parameters  $\tau_p, \nu_p, h_p$  for  $p \in \{1, \dots, P\}$ , and  $\mathbf{s} \in \mathbb{C}^{N \times 1}$  is the transmit signal, and  $\mathcal{L}(\cdot)$  is an arbitrary objective function, i.e., the  $L_2$  norm.

In the doubly-dispersive case, the parametrized channel  $\tilde{\mathbf{H}}$  is given by eq. (8), or pre-processed via leveraging the effective channel models of specific waveforms described, e.g., by eqs. (13), (16), or (19) for OFDM, OTFS and AFDM, respectively. Regardless, the underlying  $3P$ -parameter estimation problem in eq. (24) can be solved via various algorithms based on maximum likelihood, Bayesian learning, compressive sensing, and basis expansion methods [29], [30]. Such methods are most robust and realistic as the assumptions and the resolution of the former two types of methods may not be practical, and are expected to be more beneficial to the communications subsystem due to the underlying joint estimation of the channel coefficients.

## V. KEY PERFORMANCE INDICATOR (KPI)-CENTERED COMPARATIVE ANALYSIS

In view of all the above, we finally offer a qualitative comparison of OFDM, OTFS and AFDM – respectively representing the classic, state-of-the-art (SotA) and most-recent alternative – ISAC-friendly waveforms for B5G/6G systems. To this end, we consider various relevant KPIs for communication and sensing, functions, both in terms of features and implementation aspects. The GFDM and FMCW waveforms are also included for comparison, for communications and radar sensing performances respectively.

The result is given in Table I, and while it is not possible to elaborate on all comparison points due to space limitations, we briefly elaborate on a few most important of the selected KPIs. In particular, perhaps the most important communications KPI in doubly-dispersive channels is the Doppler-shift robustness, *i.e.*, the compatibility to high-mobility and EHF conditions, which is only attained by the OTFS and AFDM waveforms due to the inherent delay-Doppler domain orthogonality. On this aspect, it is noteworthy that OTFS achieves full diversity only in finite signal-to-noise ratio (SNR) regimes converging to first order asymptotic diversity [18], while AFDM provides guaranteed full diversity generally [12] and is also known to be the only Doppler-robust waveform to achieve full diversity also in MIMO scenarios. On the other hand, due to their fundamental roots on OFDM, both AFDM and GFDM also suffer from higher peak-to-average power ratio (PAPR), whereas OTFS enjoys a low PAPR due to the DFT-based spreading of the symbol powers in the time-frequency domain. This advantage is closely linked to implementation cost and hardware stability, especially in relation to the power amplifier (PA) and radio frequency (RF) component efficiency which becomes more prominent in the massive MIMO scenarios.

Another important point to consider is the computational complexity, which is linked to various signal processing procedures such as modulation and channel estimation. In this regard, while both OTFS and AFDM can be interpreted as modified precoding schemes for OFDM transmitters, such that core OFDM modulators can be reused, the one-dimensional (1D) AFDM modulator exhibits a higher efficiency than the 2D OTFS modulator. This reduced dimension of the waveform also shows a similar advantage for channel estimation, in terms of both computational complexity and the required piloting overhead.

In terms of target sensing performance, OTFS and AFDM exhibit a significant improvement in the Doppler-domain ambiguity over OFDM, but such methods are restricted as they are not optimized for correlation as with FMCW waveforms. Therefore, super-resolution methods and on-grid estimation methods on the discrete delay-Doppler domain of the waveforms are leveraged, which can achieve extremely high resolutions compared to those of FMCW, often used in automotive radar, given sufficient parameterization<sup>13</sup> such as the carrier frequency and symbol period.

<sup>13</sup>It is expected that in B5G systems, the required parameters will be sufficiently satisfied to achieve high resolutions.

TABLE I: A comparative table of various waveforms and their ISAC KPIs, with qualitative measures: high, medium, low. The color of each cell corresponds to the relative performance measure, ranging from **green** denoting an attractive performance, **yellow**, to **red** denoting less performant.

		Key Performance Indicator	Waveform			
			OFDM	OTFS	AFDM	GFDM
Communications	Performance	Waveform Domain	Time-frequency	Delay-Doppler	Chirp	Filter-bank
		Delay Robustness	High	High	High	High
		Doppler Robustness	Low	High	High	Medium
		Peak-to-Average Power Ratio	High	Low	High	Medium
		Out-of-Band Emission Rate	High	Medium	High	Low
		Diversity in TV Channels	Low	Medium	High	Medium
		Frame Guard (CP) Overhead	High	Low	Medium	Medium
	Pilot Guard Overhead	Medium	High	Low	Medium	
	Implementation	Modulation Complexity	Low	High	Medium	High
		OFDM Compatibility	High	High	High	High
		PA Strain	High	Low	Medium	Medium
		MIMO Scalability	High	Medium	High	Medium
		EHF Feasibility	Low	High	High	Medium
		Full-Duplex Potential	Low	Medium	High	Medium
		Key Performance Indicator	OFDM	OTFS	AFDM	FMCW
Target Sensing	Performance	Delay Ambiguity	Low	Medium	<i>Variable</i>	Low
		Doppler Ambiguity	High	Medium	<i>Variable</i>	Low
		Peak-to-Sidelobe Ratio	Low	Medium	<i>Variable</i>	Low
		Range Resolution	High	High	High	High
		Velocity Resolution	Medium	High	High	High
		Max. Unambiguous Range	Medium	Medium	Medium	High
	Max. Unambiguous Velocity	Medium	Medium	Medium	High	
	ISAC Implem.	Implementation Cost	Low	Medium	Medium	Low
		Engineering Complexity	Low	Medium	Medium	Low
		MIMO Array Extendibility	High	Medium	High	High
CSI Estimation Complexity		Low	Medium	Medium	High	
ISAC Feasibility	Medium	High	High	Medium		

The above-described properties in both communications and sensing performances must be satisfied and be coherent, in order for a waveform to be considered a strong candidate for ISAC in B5G/6G. Clearly, as observed from the color scaling of Table. I, OTFS and AFDM are the most promising candidates satisfying most of the ISAC criteria, with some trade-offs between the two waveforms in terms of complexity, power and spectral efficiency, which is to be further addressed in a future work.

## VI. FUTURE WORKS

It can be seen that while OTFS and AFDM are the most promising candidates to enable high-performance ISAC for next-generation wireless networks, there are still many important topics to be

addressed in order to enable the incorporation of such techniques into future standards. Indeed, any given row of Table I – such as the PAPR of AFDM or the CSI estimation complexity of OTFS – can be a subject of optimization and development. The authors hope that this article helps the ISAC research community with fundamental insights, techniques, and future direction to promote the development of high-performance ISAC in doubly-dispersive environments for next-generation wireless networks.

## REFERENCES

- [1] T. S. Rappaport *et al.*, "Wireless communications and applications above 100 GHz: Opportunities and challenges for 6G and beyond," *IEEE Access*, vol. 7, pp. 78 729–78 757, 2019.
- [2] N.-S. Vo, T. Q. Duong, and Z. Sheng, "The key trends in B5G technologies, services and applications," *Mobile Networks and Applications*, vol. 27, no. 4, pp. 1716–1718, 2022.
- [3] H. Zhou, W. Xu, J. Chen, and W. Wang, "Evolutionary V2X technologies toward the internet of vehicles: Challenges and opportunities," *Proceedings of the IEEE*, vol. 108, no. 2, pp. 308–323, 2020.
- [4] D. W. Bliss *et al.*, *Dispersive and Doubly Dispersive Channels*. Cambridge University Press, 2013, pp. 341–364.
- [5] T. Wang, J. Proakis, E. Masry, and J. Zeidler, "Performance degradation of OFDM systems due to Doppler spreading," *IEEE Trans. Wireless. Commun.*, vol. 5, no. 6, pp. 1422–1432, 2006.
- [6] J. A. Zhang, M. L. Rahman, K. Wu, X. Huang, Y. J. Guo, S. Chen, and J. Yuan, "Enabling joint communication and radar sensing in mobile networks—a survey," *IEEE Commun. Surveys Tuts.*, vol. 24, no. 1, pp. 306–345, 2022.
- [7] Y. Zhong *et al.*, "Empowering the V2X network by integrated sensing and communications: Background, design, advances, and opportunities," *IEEE Network*, vol. 36, no. 4, pp. 54–60, 2022.
- [8] Z. Wei, W. Yuan, S. Li, J. Yuan, G. Bharatula, R. Hadani, and L. Hanzo, "Orthogonal time-frequency space modulation: A promising next-generation waveform," *IEEE Wireless Communications*, vol. 28, no. 4, pp. 136–144, 2021.
- [9] W. Anwar *et al.*, "Performance analysis of various waveforms and coding schemes in V2X communication scenarios," in *2020 IEEE Wireless Communications and Networking Conference (WCNC)*, 2020, pp. 1–8.
- [10] L. Gaudio, M. Kobayashi, G. Caire, and G. Colavolpe, "On the effectiveness of OTFS for joint radar parameter estimation and communication," *IEEE Transactions on Wireless Communications*, vol. 19, no. 9, pp. 5951–5965, 2020.
- [11] X. Ouyang *et al.*, "Orthogonal chirp division multiplexing," *IEEE Trans. Commun.*, vol. 64, no. 9, pp. 3946–3957, 2016.
- [12] A. Bemani, N. Ksairi, and M. Kountouris, "Affine frequency division multiplexing for next generation wireless communications," *IEEE Transactions on Wireless Communications*, pp. 1–1, 2023.
- [13] J. J. Healy *et al.*, *Linear canonical transforms: Theory and applications*. Springer, 2015, vol. 198.
- [14] "RP-234069: Study on channel modelling for Integrated Sensing And Communication (ISAC) for NR". *RAN Meeting #102*, Nokia Shanghai Bell, Dec. 2023.
- [15] R. Prasad, *OFDM for wireless communications systems*. Artech House, 2004.
- [16] S.-C. Pei and J.-J. Ding, "Closed-form discrete fractional and affine fourier transforms," *IEEE Trans. Sig. Proc.*, vol. 48, no. 5, pp. 1338–1353, 2000.
- [17] T. Erseghe, N. Laurenti, and V. Cellini, "A multicarrier architecture based upon the affine fourier transform," *IEEE Transactions on Communications*, vol. 53, no. 5, pp. 853–862, 2005.
- [18] G. D. Surabhi, R. M. Augustine, and A. Chockalingam, "On the diversity of uncoded OTFS modulation in doubly-dispersive channels," *IEEE Transactions on Wireless Communications*, vol. 18, no. 6, pp. 3049–3063, 2019.
- [19] T. Thaj, E. Viterbo, and Y. Hong, "Orthogonal time sequency multiplexing modulation: Analysis and low-complexity receiver design," *IEEE Transactions on Wireless Communications*, vol. 20, no. 12, pp. 7842–7855, 2021.
- [20] H. Lin and J. Yuan, "Orthogonal delay-doppler division multiplexing modulation," *IEEE Transactions on Wireless Communications*, vol. 21, no. 12, pp. 11 024–11 037, 2022.
- [21] B. Farhang-Boroujeny, "OFDM versus filter bank multicarrier," *IEEE Sig. Proc. Mag.*, vol. 28, no. 3, pp. 92–112, 2011.
- [22] N. Michailow *et al.*, "Generalized frequency division multiplexing for 5th generation cellular networks," *IEEE Transactions on Communications*, vol. 62, no. 9, pp. 3045–3061, 2014.
- [23] M. A. Richards, *Fundamentals of Radar Signal Processing*. McGraw-Hill Professional, 2005.
- [24] H. S. Rou, G. T. F. de Abreu, D. González G., and O. Gonsa, "Integrated sensing and communications for 3D object imaging via bilinear inference," *Accepted in IEEE Transactions on Wireless Communications*, 2024.
- [25] J. Li and P. Stoica, *MIMO radar signal processing*. John Wiley & Sons, 2008.
- [26] J. Zhu, Y. Tang, X. Wei, H. Yin, J. Du, Z. Wang, and Y. Liu, "A low-complexity radar system based on affine frequency division multiplexing modulation," *arXiv preprint arXiv:2312.11125*, 2023.
- [27] P. Kumari, J. Choi, N. González-Prelcic, and R. W. Heath, "IEEE 802.11ad-based radar: An approach to joint vehicular communication-radar system," *IEEE Transactions on Vehicular Technology*, vol. 67, no. 4, pp. 3012–3027, 2018.
- [28] P. Raviteja, K. T. Phan, Y. Hong, and E. Viterbo, "Orthogonal time frequency space (OTFS) modulation based radar system," in *2019 IEEE Radar Conference (RadarConf)*, 2019, pp. 1–6.
- [29] L. Gaudio, M. Kobayashi, G. Caire, and G. Colavolpe, "Joint radar target detection and parameter estimation with MIMO-OTFS," in *2020 IEEE Radar Conference (RadarConf20)*, 2020, pp. 1–6.
- [30] Y. Liu, Y. L. Guan, and D. González G., "Near-optimal BEM OTFS receiver with low pilot overhead for high-mobility communications," *IEEE Transactions on Communications*, vol. 70, no. 5, pp. 3392–3406, 2022.